Polarization scramblers with plasmonic meander-type metamaterials

Philipp Schau,[1,*] Liwei Fu,[1] Karsten Frenner,[1] M. Schäferling,[2] Heinz Schweizer,[2] Harald Giessen,[2] Luis Miguel Gaspar Venancio,[3] and Wolfgang Osten[1]

[1]*Institut für Technische Optik and Research Center SCoPE, Universität Stuttgart, Pfaffenwaldring 9, Stuttgart, Germany*

[2]*4th Physics Institute and Research Center SCoPE, Universität Stuttgart, Pfaffenwaldring 57, 70550 Stuttgart, Germany*

[3]*European Space Research and Technology Ctr., Keplerlaan 1, 2200 Noordwijk, Netherlands*

[*]*schau@ito.uni-stuttgart.de*

Abstract: Due to plasmonic excitations, metallic meander structures exhibit an extraordinarily high transmission within a well-defined pass band. Within this frequency range, they behave like almost ideal linear polarizers, can induce large phase retardation between s- and p-polarized light and show a high polarization conversion efficiency. Due to these properties, meander structures can interact very effectively with polarized light. In this report, we suggest a novel polarization scrambler design using spatially distributed metallic meander structures with random angular orientations. The whole device has an optical response averaged over all pixel orientations within the incident beam diameter. We characterize the depolarizing properties of the suggested polarization scrambler with the Mueller matrix and investigate both single layer and stacked meander structures at different frequencies. The presented polarization scrambler can be flexibly designed to work at any wavelength in the visible range with a bandwidth of up to 100 THz. With our preliminary design, we achieve depolarization rates larger than 50% for arbitrarily polarized monochromatic and narrow-band light. Circularly polarized light could be depolarized by up to 95% at 600 THz.

OCIS codes: (050.2770) Gratings; (120.6085) Space instrumentation; (160.3918) Meta-materials; (230.4170) Multilayers; (250.5403) Plasmonics; (310.5448) Polarization, other optical properties.

References and links

1. "GES DISC DAAC Data Guide: Coastal Zone Color Scanner (CZCS) Instrument Guide," http://disc.sci.gsfc.nasa.gov/oceans/documentation/scientific-documentation/CZCS_Sensor.gd.shtml.
2. S. C. McClain, R. A. Chipman, and L. W. Hillman, "Aberrations of a horizontal-vertical depolarizer," Appl. Opt. **31**(13), 2326–2331 (1992).
3. MERIS Product Handbook, Issue 3.0 (European Space Agency, 2011).
4. M. Aguirre, B. Berruti, J.-L. Bezy, M. Drinkwater, F. Heliere, U. Klein, C. Mavrocordatos, P. Silvestrin, B. Greco, and J. Benveniste, "Sentinel-3: The ocean and medium-resolution land mission for GMES operational services," ESA Bull. **131**, 24–29 (2007).
5. M. R. Dobber, R. J. Dirksen, P. F. Levelt, G. H. J. van den Oord, R. H. M. Voors, Q. Kleipool, G. Jaross, M. Kowalewski, E. Hilsenrath, G. W. Leppelmeier, Johan de Vries, W. Dierssen, and N. C. Rozemeijer, "Ozone monitoring instrument calibration," IEEE Trans. Geosci. Rem. Sens. **44**(5), 1209–1238 (2006).
6. P. F. Levelt, G. H. J. van den Oord, M. R. Dobber, A. Malkki, Huib Visser, Johan de Vries, P. Stammes, J. O. V. Lundell, and H. Saari, "The ozone monitoring instrument," IEEE Trans. Geosci. Rem. Sens. **44**(5), 1093–1101 (2006).
7. J. Valentine, S. Zhang, T. Zentgraf, E. Ulin-Avila, D. A. Genov, G. Bartal, and X. Zhang, "Three-dimensional optical metamaterial with a negative refractive index," Nature **455**(7211), 376–379 (2008).
8. R. Gordon, A. G. Brolo, A. McKinnon, A. Rajora, B. Leathem, and K. L. Kavanagh, "Strong polarization in the optical transmission through elliptical nanohole arrays," Phys. Rev. Lett. **92**(3), 037401 (2004).
9. J. Sung, M. Sukharev, E. M. Hicks, R. P. VanDuyne, T. Seideman, and K. G. Spears, "Nanoparticle spectroscopy: birefringence in two-dimensional arrays of L-shaped silver nanoparticles," J. Phys. Chem. C **112**(9), 3252–3260 (2008).

10. L. Feng, Z. Liu, V. Lomakin, and Y. Fainman, "Form birefringence metal and its plasmonic anisotropy," Appl. Phys. Lett. **96**(4), 041112 (2010).
11. S.-Y. Hsu, K.-L. Lee, E.-H. Lin, M.-C. Lee, and P.-K. Wei, "Giant birefringence induced by plasmonic nanoslit arrays," Appl. Phys. Lett. **95**(1), 013105 (2009).
12. E. Öğüt and K. Şendur, "Circularly and elliptically polarized near-field radiation from nanoscale subwavelength apertures," Appl. Phys. Lett. **96**(14), 141104 (2010).
13. A. Roberts and L. Lin, "Plasmonic quarter-wave plate," Opt. Lett. **37**(11), 1820–1822 (2012).
14. T. Li, H. Liu, S.-M. Wang, X.-G. Yin, F.-M. Wang, S.-N. Zhu, and X. Zhang, "Manipulating optical rotation in extraordinary transmission by hybrid plasmonic excitations," Appl. Phys. Lett. **93**(2), 021110 (2008).
15. L. Feng, A. Mizrahi, S. Zamek, Z. Liu, V. Lomakin, and Y. Fainman, "Metamaterials for enhanced polarization conversion in plasmonic excitation," ACS Nano **5**(6), 5100–5106 (2011).
16. E. Altewischer, C. Genet, M. P. van Exter, J. P. Woerdman, P. F. A. Alkemade, A. van Zuuk, and E. W. J. M. van der Drift, "Polarization tomography of metallic nanohole arrays," Opt. Lett. **30**(1), 90–92 (2005).
17. M. Shcherbakov, M. Dobynde, T. Dolgova, D.-P. Tsai, and A. Fedyanin, "Full Poincaré sphere coverage with plasmonic nanoslit metamaterials at Fano resonance," Phys. Rev. B **82**(19), 193402 (2010).
18. L. M. Gaspar Venancio, S. Hannemann, G. Lubkowski, M. Suhrke, H. Schweizer, L. Fu, H. Giessen, P. Schau, K. Frenner, and W. Osten, "Metamaterials for optical and photonic applications for space: preliminary results," Proc. SPIE **8146**, 81460E, 81460E-13 (2011).
19. M. R. Shcherbakov, P. P. Vabishchevich, V. V. Komarova, T. V. Dolgova, V. Panov, V. V. Moshchalkov, and A. A. Fedyanin, "Ultrafast polarization shaping with Fano plasmonic crystals," Phys. Rev. Lett. **108**(25), 253903 (2012).
20. P. Johnson and R. Christy, "Optical constants of the noble metals," Phys. Rev. B **6**(12), 4370–4379 (1972).
21. L. Fu, H. Schweizer, T. Weiss, and H. Giessen, "Optical properties of metallic meanders," J. Opt. Soc. Am. B **26**(12), B111–B119 (2009).
22. M. Totzeck, "Numerical simulation of high-NA quantitative polarization microscopy and corresponding near-fields," Optik (Stuttg.) **112**(9), 399–406 (2001).
23. L. Li, "Use of Fourier series in the analysis of discontinuous periodic structures," J. Opt. Soc. Am. A **13**(9), 1870–1876 (1996).
24. T. Weiss, N. A. Gippius, S. G. Tikhodeev, G. Granet, and H. Giessen, "Efficient calculation of the optical properties of stacked metamaterials with a Fourier modal method," J. Opt. A, Pure Appl. Opt. **11**(11), 114019 (2009).
25. G. Granet, "Reformulation of the lamellar grating problem through the concept of adaptive spatial resolution," J. Opt. Soc. Am. A **16**(10), 2510–2516 (1999).
26. P. Schau, K. Frenner, L. Fu, H. Schweizer, and W. Osten, "Coupling between surface plasmons and Fabry-Pérot modes in metallic double meander structures," Proc. SPIE **7711**, 77111F, 77111F-10 (2010).
27. R. Ritchie, "Plasma losses by fast electrons in thin films," Phys. Rev. **106**(5), 874–881 (1957).
28. H. Raether, *Surface Plasmons on Smooth and Rough Surfaces and on Gratings* (Springer, 1988).
29. P. Schau, K. Frenner, L. Fu, H. Schweizer, H. Giessen, and W. Osten, "Design of high-transmission metallic meander stacks with different grating periodicities for subwavelength-imaging applications," Opt. Express **19**(4), 3627–3636 (2011).
30. P. Schau, K. Frenner, L. Fu, W. Osten, H. Schweizer, and H. Giessen, "Sub-wavelength imaging using stacks of metallic meander structures with different periodicities," Proc. SPIE **8093**, 80931K, 80931K-8 (2011).
31. D. H. Goldstein, *Polarized Light, Third Edition*, Revised (CRC Press Inc., Taylor & Francis Group, 2010).
32. Bryan-Brown1990 G. P. Bryan-Brown, J. R. Sambles, and M. C. Hutley, "Polarisation conversion through the excitation of surface plasmons on a metallic grating," J. Mod. Opt. **37**, 1227–1232 (1990).
33. P. S. Hauge, R. H. Muller, and C. G. Smith, "Conventions and formulas for using the Mueller-Stokes calculus in ellipsometry," Surf. Sci. **96**(1-3), 81–107 (1980).
34. A. Röseler, *Infrared Spectroscopic Ellipsometry* (Akademie-Verlag, 1990).
35. M. Honma and T. Nose, "Liquid-crystal depolarizer consisting of randomly aligned hybrid orientation domains," Appl. Opt. **43**(24), 4667–4671 (2004).
36. A. Drezet, C. Genet, and T. W. Ebbesen, "Miniature plasmonic wave plates," Phys. Rev. Lett. **101**(4), 043902 (2008).
37. B. Gompf, J. Braun, T. Weiss, H. Giessen, M. Dressel, and U. Hübner, "Periodic nanostructures: spatial dispersion mimics chirality," Phys. Rev. Lett. **106**(18), 185501 (2011).
38. L. Fu, P. Schau, K. Frenner, W. Osten, T. Weiss, H. Schweizer, and H. Giessen, "Mode coupling and interaction in a plasmonic microcavity with resonant mirrors," Phys. Rev. B **84**(23), 235402 (2011).

1. Introduction

The polarization state of light is one of the most important properties for many optical applications such as liquid-crystal displays (electro-optic effect), optical isolators (Faraday effect) or optical switches (Kerr effect). However, in some instances, such as earth observation from space, any exhibited polarization of the light is undesirable and depolarization of the light is critical for a good optical performance of a space-based instrument. One approach towards depolarizers are so called polarization scramblers or pseudodepolarizers, which divide the incident light beam into a large number of varying and

intermixed polarization angles instead of truly depolarizing the light. Currently and historically, most pseudodepolarizers in space instruments utilize different arrangements of birefringent wedges.

The horizontal-vertical (HV) depolarizer, one of the first pseudodepolarizers launched to space, consists of two birefringent wedges with their fast axes perpendicular to each other and has been used in NASA's Coastal Zone Color Scanner (CZCS) on NIMBUS 7 platform [1]. This device scrambles linearly and circularly polarized light. However, linear polarization states rotated by 45 or 135 degrees are left unchanged [2]. Another wedge-type depolarizer currently used onboard Envisat in the MEdium Resolution Imaging Spectrometer (MERIS) [3] and onboard Sentinel-3 in the Ocean and Land Color Instrument (OLCI) [4] uses two birefringent quartz wedges and an additional fused silica wedge for chromatic correction. In this case, all polarization states can be depolarized but strong and fast spectral oscillations are introduced in the residual polarization. In order to detect weak spectral lines, these fast spectral oscillations must be minimized. For accurate measurements of the NO_2 level in the atmosphere, for instance, local changes in the intensity spectrum of only 0.1% have to be distinguished. To reduce the spectral oscillations, a Dual Babinet scrambler consisting of four birefringent wedges is used onboard Aura in the Ozone Measuring Instrument (OMI). It introduces only slow (long-range) spectral oscillations, which is beneficial but converges the beam slightly [5,6].

All pseudodepolarizers described above are applicable in the visible and UV part of the electromagnetic spectrum and need a minimum wavelength bandwidth of about 100 nm to depolarize the incident light completely. Major drawbacks of these designs are their bulkiness and, hence, heavy weight as well as their limitation in size. For instance, all polarization scramblers implemented in the European Space Agency (ESA) missions have a size smaller than 40 mm since birefringent materials (e.g. quartz, MgF_2, Al_2O_3) with larger dimensions may break under thermal stress due to the anisotropy of their thermal expansion coefficient.

Especially for space instruments, large-area and low-weight optical elements are desirable. This is where metamaterials come into play - artificial structures with unusual optical properties not observed in the constituent materials and not readily available in nature [7]. Such materials could advantageously replace bulky standard optical components by a thin layer to achieve the same functionality but with higher efficiency and a lower mass and volume. Large birefringence and plasmonic anisotropy have been demonstrated in plasmonic metamaterials [8–17]. Therefore, the polarization state of light can be manipulated effectively, depending on the size and shape of the metallic nanostructures [8–10]. They can be used to realize phase retarders [9–13], polarization rotators [14] or polarization converters [15] by using structured thin metallic layers. Depolarization effects in metamaterials have also been discussed frequently [16,17]. However, a metamaterial pseudodepolarizer has, to our knowledge, not been investigated yet.

In this contribution we demonstrate a metamaterial-based polarization scrambler that could be used for earth observation from space in the wavelength range between 400 nm and 1000 nm [18]. The proposed device is based on metallic meander structures, works in transmission and can depolarize linearly and circularly polarized light simultaneously within a pass band. These depolarization properties are attributed to the peculiar optical properties of the meander structure, which behaves not only like an almost ideal linear polarizer, but also demonstrates a large phase retardation and polarization conversion capability between two orthogonal polarization states [19].

2. Numerical simulation models and analysis methods

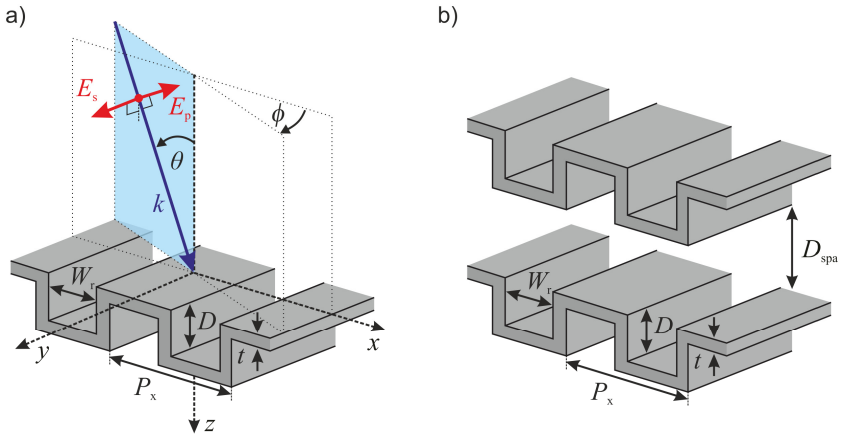

Fig. 1. (a) The meander structure is defined by the geometrical parameters thickness t, corrugation depth D, ridge width W_r and periodicity P_x. (b) For a double meander structure, the distance between the two sheets is defined as D_{spa}.

The investigated polarization scrambler is basically a plasmonic metamaterial consisting of thin metal films corrugated on both sides with a thickness t, a corrugation depth D and a periodicity P_x (Fig. 1(a)). To achieve inversion symmetry along the propagation direction of the incident light for high transmission, the condition $W_r = P_x/2 - t$ has to be fulfilled, where W_r is the ridge width. If two meander structures are stacked onto each other (Fig. 1(b)), the distance between them is labeled D_{spa}. For simplicity, shifts between the two meander surfaces are not considered. Silver is our material of choice due to its low absorption in the whole visible region. The dielectric function was derived from the Drude model and should be complemented with material data of Johnson and Christy [20] if higher frequencies are of interest. We used the plasma frequency $\omega_p = 1.37 \times 10^{16}$ rad/s and the scattering frequency $\nu = 8.5 \times 10^{13}$ rad/s [21] for deriving the dispersion of Ag. Both the single and double meander structure are placed in vacuum although another permittivity configuration can be easily obtained. For numerical calculations we used Microsim, an in-house simulation package, which employs the rigorous coupled-wave analysis (RCWA) [22] improved by factorization rules [23]. We consider at least 100 positive Fourier modes, which provide a reasonable trade-off between accuracy and computation time. Eventually, the results were verified with another RCWA package combined with adaptive spatial resolution [24,25].

3. Properties of meander structures

When p-polarized light is incident onto a thin meander structure, two kinds of surface plasmon polaritons (SPP) are excited at the metal-dielectric interfaces, namely short range surface plasmon polaritons (SRSPP) and long range surface plasmon polaritons (LRSPP) [21]. The SRSPP represents the symmetric and low-frequency mode whereas the LRSPP corresponds to the antisymmetric and high-frequency case. They can be identified by their respective field distributions [21,26] or by varying the thickness of the metal film [27,28]. It was found that with certain meander geometries, plasmon resonances induce a high-transmission pass band, which is bounded by two Fano-type resonances (Fig. 2(a)) [21,29]. This high-transmission pass band is the main reason for using meander structures for the proposed depolarizer. Other plasmonic nanostructures such as nanowire arrays show a stop band behavior, while nanoslit arrays or nanohole arrays exhibit only one narrow and low-transmission pass band induced by a single resonance [9,16,17].

A dispersion diagram as a function of the in-plane wave vector $k_x/K_g = \sin\theta\, k_0/K_g$, where k_0 is the wave vector in free space and $K_g = 2\pi/P_x$ the reciprocal lattice vector, is shown in Fig.

2(b). Besides highlighting the particular plasmon frequencies by the extinction maxima (-ln(T)), this figure also shows that the same pass band exists for light incident at oblique angles.

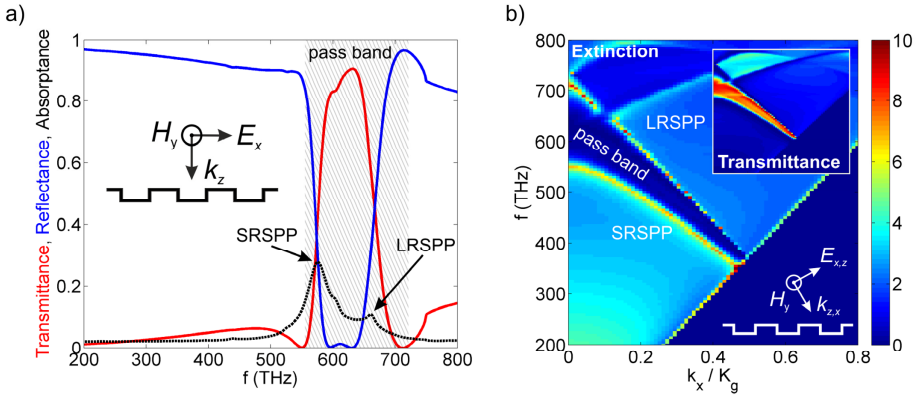

Fig. 2. (a) Transmittance, reflectance and absorptance spectra of a single meander structure (t = 30 nm, D = 40 nm, P_x = 400 nm) at perpendicular incidence. (b) Dispersion diagram (extinction, -ln(T)) of the same structure. The k_x axis is scaled by the reciprocal lattice vector $K_g = 2\pi/P_x = 1.57 \times 10^5$ cm^{-1}. The pass band between the SRSPP (550 THz) and LRSPP (710 THz) modes occurs via interaction of two Fano-type resonances. The inset located in the upper-right corner shows the transmittance of the same structure with a color scale ranging from 0 to 1.

Our previous studies have demonstrated how the SRSPP and LRSPP frequencies influence the shape of the pass band and how they can be shifted by geometry variation [30]. By decreasing the thickness t of the meander structure, the SRSPP mode decreases in frequency whereas the LRSPP mode remains almost constant. The increase of the meander depth D at a constant thickness t and periodicity P_x leads to a down-shift of the SRSPP frequency, while the LRSPP mode experiences only a slight red-shift. Finally, with all other geometrical parameters fixed, the SRSPP and LRSPP frequencies are decreased at larger periodicities P_x although with different slopes. To sum up, by changing the geometrical parameters, we can design meander structures in such a way that extraordinarily high transmission can be achieved at any frequency in the visible and near infrared ranges. Hence, polarization scramblers that consist of spatially distributed meander structures can be flexibly tuned to any optical frequency in the same way.

4. Jones and Mueller matrices of single meander structures at normal incidence

In order to characterize the polarization properties of the meander structure, we use the Stokes vector representation. The Stokes vector consists of four Stokes parameters S_i (i = 0-3), which describe the intensity and polarization of a beam of light [31]. After interaction with any optical component, which can be described by the corresponding Mueller matrix, the emerging light beam is characterized by a new set of Stokes parameters S_i' (i = 0-3). This way, S_i' can be expressed as a linear combination of the four Stokes parameters of the incident beam (S_i). Using the Mueller matrix expression, these equations are written as:

$$\begin{bmatrix} S_0' \\ S_1' \\ S_2' \\ S_3' \end{bmatrix} = \begin{bmatrix} m_{00} & m_{10} & m_{20} & m_{30} \\ m_{10} & m_{11} & m_{21} & m_{31} \\ m_{20} & m_{12} & m_{22} & m_{32} \\ m_{30} & m_{13} & m_{23} & m_{33} \end{bmatrix} \cdot \begin{bmatrix} S_0 \\ S_1 \\ S_2 \\ S_3 \end{bmatrix}. \quad (1)$$

A depolarizer or polarization scrambler transfers energy from polarized states into depolarized states. The Mueller matrix of a pure non-uniform partial depolarizer is given by

$$\mathbf{M}_{\text{partial}} = \begin{bmatrix} 1 & 0 & 0 & 0 \\ 0 & a & 0 & 0 \\ 0 & 0 & b & 0 \\ 0 & 0 & 0 & c \end{bmatrix}, \tag{2}$$

where $a \neq b \neq c$ and a, b, $c < 1$. For $a = b = c \neq 0$, the system is called a pure uniform depolarizer and if $a = b = c = 0$, the incident polarized light will be completely depolarized (ideal depolarizer) [31]. To obtain a perfect polarization scrambler, the degree of polarization P′ has to be minimized. P′ is calculated by dividing the intensity of the polarized part of the light (I'_{pol}) by the total light intensity (I'_{tot})

$$P' = \frac{I'_{pol}}{I'_{tot}} = \frac{\sqrt{S_1'^2 + S_2'^2 + S_3'^2}}{S_0'}. \tag{3}$$

Before the complete Mueller matrices of meander structures in dependence of the incidence and azimuth angles are presented, its optical properties at normal incidence will be analyzed using the Jones formalism [31]. This helps us to gain a physical insight into the polarization properties of a single meander structure and to better understand why meander structures can be used to depolarize light effectively.

First, the transmittance of p- and s-polarized light of a single meander structure with P_x = 400 nm, D = 40 nm and t = 30 nm was numerically calculated at normal incidence in dependence of the azimuth angle ϕ for the frequencies 600 THz, 630 THz and 650 THz, respectively (Fig. 3(a)). For the investigated meander structure, these frequencies are located within the pass band, where 600 THz is at the low-frequency edge, 630 THz in the center and 650 THz at the high-frequency edge of the pass band. At $\phi = 0°$, s-polarized light is blocked to a large extent, whereas p-polarized light is transmitted, which is the typical behavior of a linear polarizer. Increasing the azimuth angle towards $\phi = 90°$ increases the transmittance of the s-polarized light up to a state close to total transmission.

Secondly, Fig. 3(b) shows different degrees of phase retardation δ between p- and s-polarized light at arbitrary azimuth angles and at the same frequencies. It is interesting to note that at 600 THz almost no phase shift and, hence, no phase retardation occurs. Furthermore, at 650 THz, where the transmittance is still as high as 80%, a phase retardation $\delta = 130°$ can be obtained. Similar to metallic gratings [32], the meander structure is also capable to convert polarization to a large degree, i.e. a fraction of the incident p-polarized light is absorbed and re-radiated as s-polarized light and vice versa. Figure 3(c) shows the polarization conversion transmittance from s- to p-polarized light in dependence of the azimuth angle ϕ for the same frequencies as before. The polarization conversion follows closely a $\sin^2(2\phi)$ function [32] and has its maximum at an angle of $\phi = 45°$. The conversion is stronger at higher frequencies where the phase retardation is larger as well.

In order to describe the meander structure analytically, we use the same formalism as the authors in [17] for a plasmonic nanoslit metamaterial at Fano resonance. For an anisotropic medium under normal incidence with the optical axis oriented along the x-coordinate of the Cartesian laboratory system, its Jones matrix can be expressed as:

$$\mathbf{J}_{\text{anisotropic}} = \begin{bmatrix} Ae^{i\psi} & 0 \\ 0 & B \end{bmatrix}. \tag{4}$$

A and B are the amplitudes of the transmission coefficients for p- and s-polarized light, respectively, and ψ the induced phase delay at $\phi = 0°$ between them. At an arbitrary azimuth angle ϕ one obtains the Jones matrix for a meander structure by applying unitary rotation transformation:

$$\mathbf{J}_{\text{meander}}(\phi) = R(\phi)\begin{bmatrix} Ae^{i\psi} & 0 \\ 0 & B \end{bmatrix} R(-\phi)$$
$$= \begin{bmatrix} Ae^{i\psi}\cos^2\phi + B\sin^2\phi & B\cos\phi\sin\phi - Ae^{i\psi}\cos\phi\sin\phi \\ B\cos\phi\sin\phi - Ae^{i\psi}\cos\phi\sin\phi & Ae^{i\psi}\sin^2\phi + B\cos^2\phi \end{bmatrix} \quad (5)$$

with the rotation matrix

$$R(\phi) = \begin{bmatrix} \cos\phi & \sin\phi \\ -\sin\phi & \cos\phi \end{bmatrix}. \quad (6)$$

With Eq. (5) we can now describe the amplitude, phase retardation and polarization conversion of meander structures, which is shown in Fig. 3(a)-3(c). The p- and s-polarized transmittance spectra (Fig. 3(a)) correspond to the squared absolute values of J_{pp} and J_{ss} of $\mathbf{J}_{\text{meander}}$, respectively. In Fig. 3(a) the fit curves for the s-polarized spectra are shown with the values for A, B and ψ given in the figure caption. The fitting results for the p-polarized transmittance spectra are not shown because they can be obtained easily due to the structure's symmetry. The model also describes the phase retardation and polarization conversion using the same fitting parameters, although there are two Fano resonances involved instead of one compared to [17] (Fig. 3(b),3(c)). Note that the meander structure has a similar transmission for the three frequencies but different phase retardation and polarization conversion efficiency. This indicates different depolarization degrees P´ when used for designing a polarization scrambler.

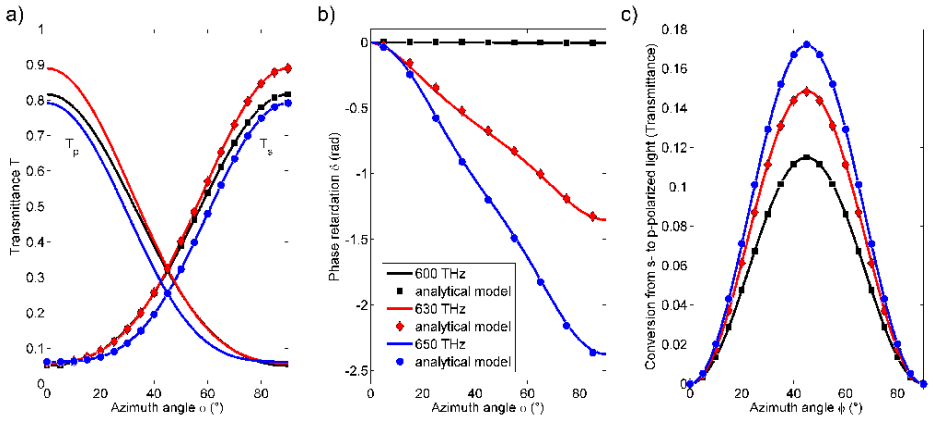

Fig. 3. (a) Transmittance spectra of p-polarized (T_p) and s-polarized light (T_s) as a function of the azimuth angle ϕ at normal incidence for f = 600 THz, 630 THz and 650 THz. The fit curves are indicated by markers and were obtained by calculating $|J_{pp}|^2$ or $|J_{ss}|^2$ from Eq. (5) respectively. The fit parameters for 600 THz were A = 0.9, B = 0.23 and ψ = 0.005, for 630 THz A = 0.94, B = 0.24 and ψ = 0.67 and for 650 THz A = 0.89, B = 0.25 and ψ = 1.19 (b) Phase retardation δ as a function of the azimuth angle ϕ. The changes agree well with the analytical model from Eq. (5) (arg(J_{pp})-arg(J_{ss})). For different frequencies in the pass band, δ has different slopes. (c) Transmittance of p-polarized light as a function of the azimuth angle ϕ for incident s-polarized light $|J_{ps}|^2$ or $|J_{sp}|^2$, respectively. The investigated meander structure has the same geometry parameters as the one in Fig. 2 (P_x = 400 nm, D = 40 nm, t = 30 nm).

The good agreement between the model and the numerical results suggests that other plasmonic metamaterials such as plasmonic nanoslits might be well suited for the proposed depolarizer. However, as pointed out before, the main difference is the combination of high transmission and the broad pass band induced by two Fano resonances instead of one.

Since the single meander structure itself is not capable of depolarizing light, its Mueller matrix can be calculated from the Jones matrix via the Jones-Mueller matrix transformation [33,34]:

$$\mathbf{M}_{\text{meander}} = \mathbf{A}^{+}\left(\mathbf{J}\otimes\mathbf{J}^{*}\right)\mathbf{A} \tag{7}$$

with

$$\mathbf{A} = \frac{1}{\sqrt{2}}\begin{bmatrix} 1 & 1 & 0 & 0 \\ 0 & 0 & 1 & -i \\ 0 & 0 & 1 & i \\ 1 & -1 & 0 & 0 \end{bmatrix}. \tag{8}$$

The main idea of our approach towards a polarization scrambler is that meander structures are spatially distributed in tiles on a surface. Each meander structure within such a tile is rotated by a random angle. The size of the tiles and hence the number of the tiles within the beam spot of the incident light is chosen in such a way that an averaged optical response with a maximum depolarization degree is achieved, similar to the working principle of liquid-crystal depolarizers [35,36]. Using the coordinate system shown in Fig. 1(a), we can arrange the tiles by rotating the azimuth angle ϕ randomly and integrate Eq. (7) over ϕ from 0 to π (due to their C2 symmetry) with the same weighting factor for each element and angle ϕ. In our numerical simulations we found that the results of 30 adjacent meander unit cells are very close to the ones of an infinite grating. With square-shaped meander tiles, this would mean an area of at least 144 μm^2 with the currently investigated structure (P_x = 400 nm). However, due to diffraction effects, the final patch size should be larger [35]. Please note that the incidence angle θ can be used as well for such an averaging process [36]. In the case of earth observation, however, the light is paraxial and perpendicularly incident.

Using the Jones matrix elements from Eq. (5) along with the fit parameters A, B and ψ from Fig. 3(a)-3(c), the Mueller matrices of the single meander structure at 600 THz, 630 THz and 650 THz can be easily calculated analytically. The results are shown below:

$$\mathbf{M}_{600\text{THz}} = \begin{bmatrix} 1 & 0 & 0 & 0 \\ 0 & 0.74 & 0 & 0 \\ 0 & 0 & 0.73 & 0 \\ 0 & 0 & 0 & 0.47 \end{bmatrix}, \mathbf{M}_{630\text{THz}} = \begin{bmatrix} 1 & 0 & 0 & 0 \\ 0 & 0.69 & 0 & 0 \\ 0 & 0 & 0.68 & 0 \\ 0 & 0 & 0 & 0.37 \end{bmatrix}, \mathbf{M}_{650\text{THz}} = \begin{bmatrix} 1 & 0 & 0 & 0 \\ 0 & 0.61 & 0 & 0 \\ 0 & 0 & 0.60 & 0 \\ 0 & 0 & 0 & 0.21 \end{bmatrix}. \tag{9}$$

It can be seen that all off-diagonal Mueller matrix elements are zero whereas the diagonal elements are reduced to values below one. For increasing frequencies within the pass band, the diagonal elements decrease. A reason for this behavior is the larger phase retardation and polarization conversion efficiency (Fig. 3(b), 3(c)). Most importantly, pure partial depolarization for light with any polarization states is achieved at normal incidence in transmission. In contrast, pseudodepolarizers made of randomly arranged liquid crystal domains or linear polarizers cannot depolarize circularly polarized light. Some other metamaterials can only depolarize light at oblique incidence [37]. Nevertheless, only perpendicular incidence was investigated and the results can be further improved if the distribution of tiles with specific rotation angles is weighted differently.

5. Polarization scramblers using single and double meander structures

5.1 Single meander structures

In this section, the Mueller matrices of the meander structure are derived from full numerical calculations similar to the way presented in the previous section. Only this time, instead of

using the model from Eq. (5), the transmission coefficients of p- and s-polarized light as well as the polarization conversion from p- to s-polarized light and vice versa are calculated rigorously for each incidence angle θ and azimuth angle ϕ. From these transmission coefficients, we can derive the Jones matrix and subsequently calculate the Mueller matrix of a meander structure via the Jones-Mueller transformation (Eq. (7)).

We present the Mueller matrices of both single and double layer meander structures as a function of the incidence angle θ and azimuth angles ϕ at 600 THz and 650 THz, respectively. The incidence angle θ is varied from 0° to 46° and the azimuth angle ϕ from 0° to 180° in steps of 2°, respectively. The calculation is performed for the same meander structure used in Fig. 3. This geometry has been optimized for obtaining a well-defined pass band with a high transmission between 580 THz and 650 THz (Fig. 4(a)). Note that the transmittance spectra shown in Fig. 4(a) and Fig. 5(a) are for perpendicular incidence and p-polarized light only. Since s-polarized light is almost completely blocked by the meander structure, the transmittance of the proposed polarization scrambler is approximately half of the one shown in Fig. 4(a). The corresponding Mueller matrix for 600 THz is shown in Fig. 4(b). Each of the Mueller matrix elements m_{ij} is normalized to m_{00} and plotted as a function of $\sin(\theta)\cos(\phi)$ in x-direction and $\sin(\theta)\sin(\phi)$ in y-direction, respectively.

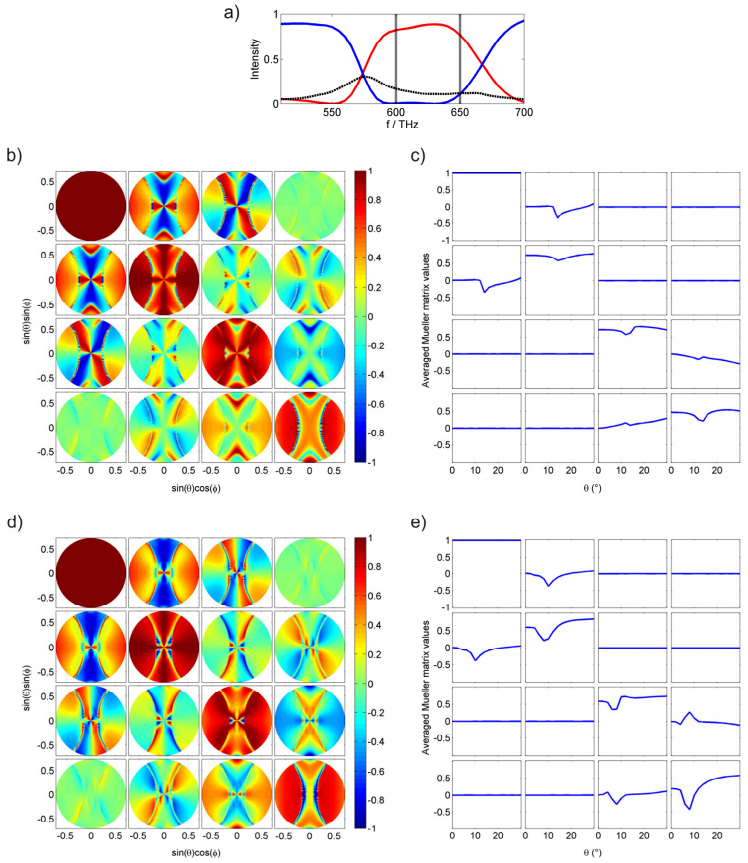

Fig. 4. (a) Spectrum of a single meander layer with period P_x = 400 nm, corrugation depth D = 40 nm and metal layer thickness t = 30 nm (b,d) Mueller matrix (elements m_{ij} with row index i = 0-3 from left to right and column index j = 0-3 from top to bottom) of the same structure at 600 THz and 650 THz, respectively. (c,e) Mueller matrix elements from (b) and (d) averaged over the azimuth angle ϕ from 0° to 180°.

One observes that the off-diagonal matrix elements have alternating positive and negative values varying with ϕ, which is related to the C2 symmetry of the meander structure. As a result, the off-diagonal elements should approach zero when the azimuth angle ϕ is averaged from 0° to 180°. Using the numerical values from Fig. 4(b), we can create a more comprehensible plot that shows the averaged Mueller matrix values as a function of the incidence angle θ (Fig. 4(c)).

It turns out that all off-diagonal elements are zero for small incidence angles $\theta < 5°$. The remaining diagonal Mueller matrix elements are reduced to $m_{11} = 0.74$, $m_{22} = 0.73$ and $m_{33} = 0.47$ and represent direct measures for the depolarization capabilities for various polarization states. For horizontally or vertically linearly polarized (LP) incident light (S = [1, ± 1, 0, 0]), the degree of polarization is $P'_{LP} = m_{11} = 0.74$ according to Eq. (3). Hence, the single meander structure depolarizes linearly polarized light by 26% within a range of $\theta < 5°$. For the same range of θ, ± 45° linearly polarized (LP45) light (S = [1, 0, ± 1, 0]) can be depolarized by 27% ($P'_{LP45} = m_{22} = 0.73$). Left-hand or right-hand circularly polarized (CP) light (S = [1, 0, 0, ± 1]) is depolarized by 53% ($P'_{CP} = m_{33} = 0.47$).

The diagonal elements of the Mueller matrix can be further reduced by shifting the operation regime to higher frequencies in the pass band due to the larger phase retardation and polarization conversion effect. For instance, at 650 THz the transmittance is still 80% as shown in Fig. 4(a) but the diagonal elements were reduced to $m_{11} = 0.6$, $m_{22} = 0.6$ and $m_{33} = 0.2$ for $\theta < 5°$ (Fig. 4(d),4(e)). Correspondingly, LP, LP45 and CP light can be depolarized by 40%, 40% and 80%. Moving to even higher frequencies, the values of the Mueller matrix elements could be further reduced, however, the transmission would be lower. The further reduction of the diagonal elements at higher frequencies can be attributed to the stronger polarization conversion between s- and p-polarized light as shown before in Fig. 3(c).

5.2 Double meander structures

In order to increase the polarization conversion effect and to achieve larger phase retardation between p- and s-polarized light in the pass band, which would yield further reduced diagonal elements, stacked meander structures are investigated in this section. As known from the properties of resonantly coupled double meander layers [26], strong interactions occur between surface plasmons and Fabry-Pérot (FP) cavity modes and between the different surface plasmon modes at smaller cavity length. The system can be understood as an FP-cavity with frequency selective mirrors (meander structures) with a cavity length of D_{spa} [38]. Within cavity lengths where the two layers are weakly coupled (e.g. at D_{spa} = 600 nm), the phase shift with ϕ is doubled compared to single meander structures.

Figure 5(a) shows the spectra of a double layer structure using the same meander structure as in the previous section with a cavity length of D_{spa} = 600 nm. The Mueller matrix of this structure resembles that of the single layer meander structure shown in Fig. 4, except that the C2-symmetry becomes more pronounced. A stronger and broader variation of the diagonal elements with ϕ can be observed (Fig. 5(b)). These effects can further reduce the diagonal elements down to $m_{11} = 0.5$, $m_{22} = 0.5$, and $m_{33} = 0.05$ for $\theta < 5°$ at 600 THz (Fig. 5(c)), compared to those of the single layer structure. This yields depolarization rates of 50%, 50% and 95% for LP, LP45 and CP light, respectively. At the higher-frequency edge of the pass band at 650 THz, the diagonal elements are further reduced to $m_{11} = 0.4$, $m_{22} = 0.4$, and $m_{33} = -0.3$ for $\theta < 5°$. The corresponding depolarization rates for LP, LP45 and CP light are 60%, 60% and 70%, respectively (Fig. 5(d),5(e)).

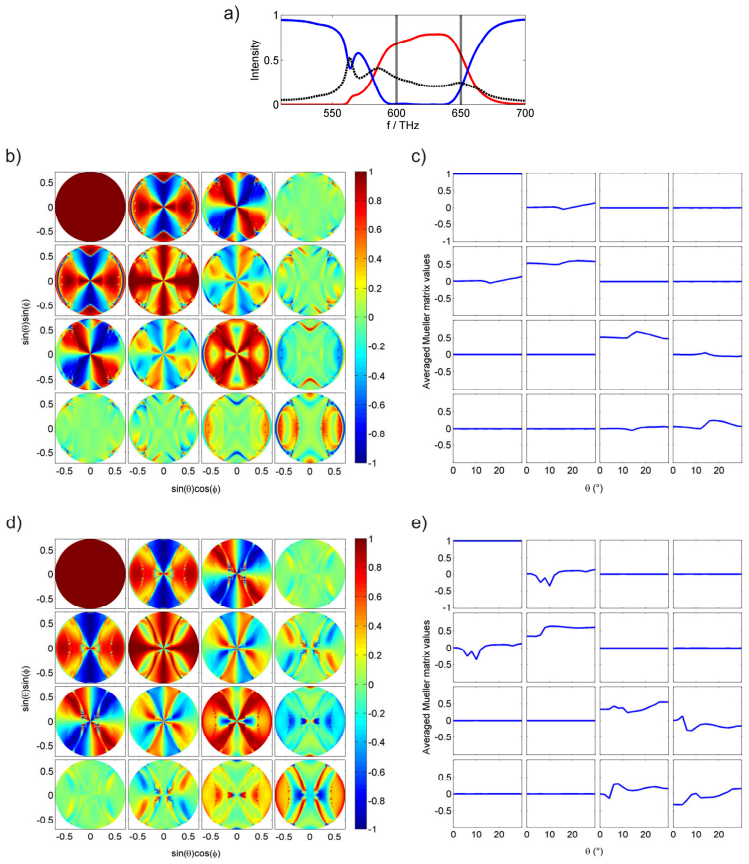

Fig. 5. (a) Spectrum of a double meander structure with period P_x = 400 nm, corrugation depth D = 40 nm, thickness t = 30 nm and spacer thickness D_{spa} = 600 nm. (b,d) Mueller matrix (elements m_{ij} with row index i = 0-3 and column index j = 0-3) of the same structure at 600 THz and 650 THz, respectively. (c,e) Mueller matrix elements from (b) and (d) averaged over the azimuth angle ϕ from 0° to 180°.

These preliminary results of the polarization scramblers employing double meander structures show that at least 60% of any polarized light can be depolarized at 650 THz. Some polarization states can be depolarized more efficiently. The meander structure investigated in Fig. 5(c), for instance, scrambles circularly polarized light most efficiently with a depolarization rate of 95% at 600 THz. Considering the multiple degrees of freedom we have, larger depolarization effects could be achieved with further optimized meander geometries. At least, the diagonal elements can be further reduced by stacking even more meander structures onto each other. However, this comes with a sacrifice in transmission, since the final transmittance would be T^n, in which n is the layer number and T is the transmittance of a single meander sheet.

6. Conclusion

We have shown numerically that polarization scramblers can be realized using metallic meander structures. These meander structures exhibit prominent optical properties such as almost ideal linear polarization, large phase retardation and high polarization conversion efficiency due to the excitation and interaction of two surface plasmon polaritons. Furthermore, we have shown that these polarization properties dependent on the azimuth angle can be described analytically by a matrix formulation for an anisotropic material that is rotated at normal incidence. The averaged off-diagonal Mueller matrix elements of a

polarization scrambler consisting of spatially distributed meander structures rotated by a random angle can be brought to zero for low incidence angles. At the higher frequency edge of a double meander pass band we obtained depolarization rates larger than 60% for both linearly and circularly polarized light.

It is notable that we can design the presented scrambler according to particular requirements just by geometry variation. Left or right circularly polarized monochromatic light for instance could even be depolarized by 95% in our numerical simulation. With further optimization, the presented polarization scrambler might be a good alternative to existing approaches and would be especially desirable for space applications due to its low weight and large-scale manufacturability. Compared to pseudodepolarizers currently used in space applications for earth observation the narrow bandwidth of our polarization scrambler is disadvantageous. On the other hand, since polarization scramblers using meander structures can be designed to perform at any optical wavelength in the visible and near infrared spectrum, they might prove advantageous for optical setups with monochromatic light sources.

Ultrafast polarization conversion in the infrared was recently shown experimentally for structures similar to the ones investigated in this report [19]. The presented depolarizer structure can be manufactured on a large scale using nano-imprint lithography.

Acknowledgments

The results presented in this paper were achieved in the frame of ESA's General Studies Programme (GSP) contract 4200022943/10/NL/AF. This work was supported by the German Research Foundation (DFG) within the funding programme Open Access Publishing. The authors also thank J. Caron and J. L. Bézy of ESTEC, Noordwijk, and T. Weiß of MPI for Light, Erlangen, for their valuable contributions.